encit 2020

ABCM
Associação Brasileira de Engenharia e Ciências Mecânicas

18th Brazilian Congress of Thermal Sciences and Engineering
November 16–20, 2020 (Online)

ENC-2020-714
Start-up Flow Visualization of Viscoplastic Fluid in Horizontal Pipes Geometries Using Particle Image Velocimetry

Angel De J. Rivera Jimenez
Vitor Yoshiharu Urazaki
Yamid J. Garcia Blanco
Eduardo Matos Germer
Admilson T. Franco
Federal University of Technology-Paraná - UTFPR, Research Center for Rheology and Non-Newtonian Fluids - CERNN,81280-340, Rua Deputado Heitor Alencar Furtado 5000 - Ecoville, Curitiba-PR, Brazil
angeljimenez@alunos.utfpr.edu.br, vitura.1998@alunos.utfpr.edu.br, yamidblanco@alunos.utfpr.edu.br, eduardomg@utfpr.edu.br, admilson@utfpr.edu.br

Abstract. *The viscoplastic fluid flows through pipelines can be found in several industrial processes, such as polymer extrusion, food pumping, and drilling of oil wells. The gel-like state of these fluids inside the pipelines after flow interruptions, represents in some situations a relevant challenge, such as the case of transportation of crude in the oil industry, due to this phenomenon increases the minimum pressure necessary to start-up the flow. However, there are not enough experimental studies focused on the relationship between the minimum pressure drop and the breaking mechanisms in the transient start-up flow. This paper presents an experimental study of transient start-up flow of viscoplastic fluids in two different horizontal pipe configurations: a straight section and an abrupt contraction arrangement (1.85 contraction ratio). An ultrasound gel solution with 30 and 20 wt% composed by Carbopol® 940 are used as a viscoplastic fluid, characterized by the Herschel-Bulkley model. Particle Image Velocimetry (PIV) is used as a visualization technique to obtain detailed measurements of mean velocity and deformation maps in the transient start-up flow. A previous stage for validation of the methodology used with the PIV technique was performed for pure glycerine in a straight tube at laminar flow conditions, and the data were compared with the analytical solution for velocity in transient flow regime for a Newtonian fluid. For the viscoplastic flow through both configurations it was possible to observe three different flow regimes: solid (plug-like), solid-fluid, and fluid. In both geometries and as the forcing of the flow gradually increases, the yielding appears through a transition. The deformation states are greater in abrupt contraction and are coupled with the wall slip phenomenon. The wall shear stress increases with external forcing, that is, with the Reynolds number. The slip velocity increases as a function of the wall shear stress and is higher for the straight section. The results show that the elastic effect plays an important role in the initial phase of destructuring of solid regime, and that the variation of Reynolds number has an influence on the elastic behavior of the material.*

Keywords: *Viscoplastic fluid, start-up flow, yielding process, wall slip, PIV*

1. INTRODUCTION

The viscoplastic fluids are used in several major industries, from a practical perspective, such materials have found an increasing number of applications, which include foods, cosmetics, oil field, etc (Alba and Frigaard, 2016; Burfoot *et al.*, 2009). Also, they are encountered in daily life in various forms such as hair gels, emulsions, food pastes, and mud (Fryer *et al.*, 2006; Cole *et al.*, 2010). Understanding the flows of viscoplastic fluids is important in practical settings including industrially relevant flows of waxy crude oils, debris flows, and flows in the food industry (Phillips *et al.*, 2011; Coussot and Meunier, 1996; Curran *et al.*, 2002).

After interruptions in some production activities, whether for operational or emergency reasons, the fluid at rest in the pipeline shows gel-like behavior (El-Gendy *et al.*, 2012).Such is the case of waxy crude oil that, when exposed to a cold environment during transport through long pipelines, it loses heat and, due to its waxy composition, a gel-like structure is formed (Sierra *et al.*, 2016). Under such conditions, restarting the flow may present some risks, as the pumping system needs to provide the pressure necessary to break the gel structure and resume the flow, called the start-up pressure, and in general, this pressure is higher than the operational one due to the viscoplasticity of the fluid.

The viscoplastic fluids behave a solid-like when the shear stress is below the yield stress (τ_y) (Dalla *et al.*, 2019), but they flow when the shear stress exceeds the τ_y value. Considering that the minimum pressure for the start-up flow is correlated with the yield stress of material (Coussot, 2014), large number of studies devoted to the yielding of viscoplastic fluids in rheometric flows have been performed (Roberts and Barnes, 2001; Putz and Burghelea, 2009; Møller *et al.*, 2009; Benmouffok-Benbelkacem *et al.*, 2010), contrary to the few numbers of experimental studies focused on the start-up visualization. Experimental studies performed by Poumaere *et al.* (2014); Sierra *et al.* (2016); Huilgol *et al.* (2019) revealed the existence of three flow regimes. Initially, an elastic behavior similar to that found in solids was observed, being characterized by the dependence of stress and shear deformation. Immediately a solid-liquid state coexistence phase is observed, and finally, a completely viscous regime is reached, which is maintained in the remaining flow.

In this work, the start-up flow is studied in two pipeline configurations, the first one is a straight pipe and the second one is a straight section followed by an abrupt contraction. A flow rate equivalent to a Reynolds number was imposed, increasing the pressure on the Carbopol (20 wt% and 30 wt%) and subsequently displacing it and causing it to yield. We measured the pressure in the Carbopol and using the particle image velocimetry (PIV), the transient flow field of the fluid was studied. For the flow conditions and geometries used, the results are consistent with the yielding process described by Putz and Burghelea (2009), it was observed that the transition between the solid-like regime and the fully yielding regime is not direct, but mediated by the coexistence of a solid-liquid regime. The presence of wall slip is observed and reveals that it is a phenomenon present in the start-up viscoplastic flow, which increases with the shear stress on the wall.

2. EXPERIMENTAL SETUP AND METHODOLOGY

2.1 Fluid preparation

The fluid used in the present work is composed of Carboxyvinyl Polymer (Carbopol®). This material chosen because it is considered a model yield stress fluid, and presents a low thixotropy (Møller *et al.*, 2006), it is transparent and has stable rheological properties. For these reasons, it is commonly used in studies as a viscoplstic fluid representation (Putz and Burghelea, 2009; Pérez-González *et al.*, 2012; Ovarlez *et al.*, 2013; Liu and de Bruyn, 2018).

For fluid preparation, initially 40 kg of deionized water were weighed on a precision balance with a resolution of 0.1 g. Subsequently, 10.6 Kg of clinical gel was added, representing 20% of total weight of the mixture, then 10 g of sodium benzoate was also added to balance the pH and prevent the proliferation of bacteria, which could affect the properties of fluid. The mixture was stirred for 6 hours, to ensure homogeneity. The final fluid had a pH = 7, a density of 1014 Kg/m^3, and it was named Carbopol 20 wt%. A similar procedure was performed for the preparation of Carbopol 30 wt%, obtaining a fluid with pH = 7 and density of 1002 Kg/m^3.

2.2 Rheological characterization

A HAAKE MARS III (Modular Advanced Rheometer system) was used to characterize the rheological properties of the fluids. The geometry used was smooth concentric cylinder, with 0.051 mm gap for shear rates from 50 to 1100 s^{-1}, and cross-hatched parallel plates with 1 mm gap for rates from 0.01 to 50 s^{-1}. According to Fernandes *et al.* (2019), the wall slip effect is minimized using geometries cross-hatched parallel plates with 35 mm and 1 mm gap. Fig. 1 illustrates the shear stress as a function of shear rate obtained on the rheometer. Measurements were performed in a temperature controlled environment at 25 °C.

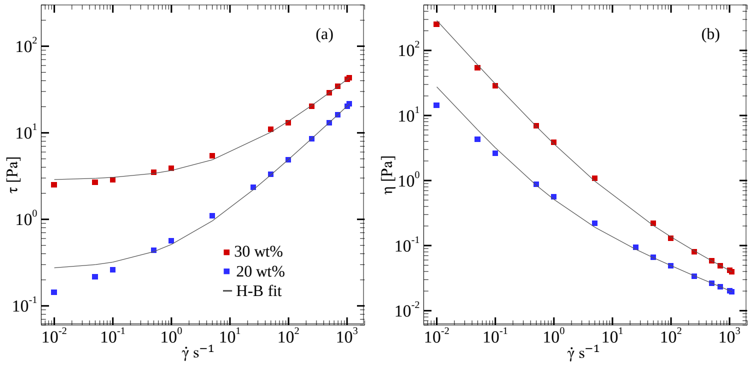

Figure 1: a) The shear stress τ and b) viscosity η behavior as a function of shear rate $\dot{\gamma}$ for each fluid. The continuous line is the Herschel-Bulkley model fit.

The data obtained with the rheometer were adjusted using the Hershel-Bulkley model, given by:

$$\tau = \tau_y + k\left(\dot{\gamma}\right)^n \tag{1}$$

where τ_y is the yield stress, n is the fluid index, and k is the consistency index. The yield stress was obtained by extrapolating the Herschel-Bulkley curve to zero shear rate. The fluid fit parameters used in this work are shown in Tab. 1.

Table 1: Yield stress and Herschel–Bulkley model parameters for the Carbopol concentrations

c [wt%]	τ_y [Pa]	n	k [Pa.s]
30	2.82	0.55	0.55
20	0.26	0.63	0.25

2.3 Experimental Setup

The present study was carried out in a hydraulic facility of acrylic tubes with 12.5 m of total length, as presented in Fig. 2. A 100 L tank (i) is used to contain the fluid and a helical rotor pump (NETZSCH mono pump) provides the flow through the pipeline (ii). For the area reduction case, an assembly of pipes with different diameters is used. The internal diameter of 25.9 mm *(D)* for the upstream zone of the contraction, and 14 mm of internal diameter *(d)* for the downstream zone. The later deals a contraction ratio of $\beta = 1.85$, where β is define as D/d. For straight pipe configuration, the internal diameter was maintained constant and equal to 25.9 mm. The flow rate is controlled by a frequency inverter (iii) with the aid of a mass flow meter (iv). Temperature and density are measured as secondary outputs of the flow meter. For a given flow rate, the total error upon the mean velocity is estimated as 1 to 3%. Pressure transmitters (v) are used along the test section, before the visualization box (vi) to obtain the entrance pressure to the system and the pressure drop measurements. The accuracy of the transmitter is estimated at 0.1% for span range (0-62 mbar) and a total error of 0.4% for the full range of measurement (0-138 bar).

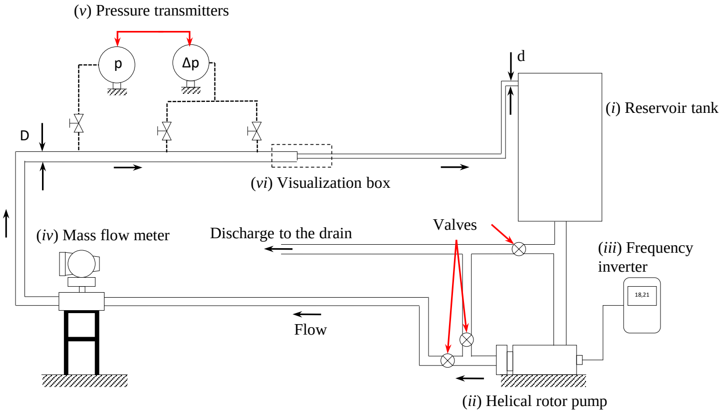

Figure 2: Hydraulic system for tests performing.

The visualization of viscoplastic flow through the flow loop is possible using a particle imaging velocimetry (PIV) technique. In this study spherical tracer particles coated by Rhodamine-B with a diameter of 10 μm were used to visualized the flow. The particles absorb light at a wavelength of 532 nm and emit it back at 560 nm. Figure 3 shows the setup for using the PIV, a laser system of 60 mJ is synchronized with a CMOS camera by a synchronization box. A visualization plane is obtained after setting the camera at 90 degrees with the laser beam.

For the experimental procedure, the fluid was placed in the 100 L tank *(i)* and then it is pumped through the flow loop system. Once the pipeline is filled, the pump *(ii)* is turned off and the fluid is left to rest for 24 hours to guarantee that any residual stress has been dissipated. After the resting time Reynolds of Re=10 and Re=100 were imposed. The Re used was set based on the Malin (1998) criterion to facilitate its control by the Lab*VIEW* platform. The Reynolds number is defined by the Eq. (2):

$$Re = \frac{\rho \bar{U}^{2-n} D^n}{k(0.75 + 0.25/n)^n 8^{n-1}} \tag{2}$$

where ρ is the density, $\bar{U}$ is the mean velocity, D is the diameter, and k and n depend on the rheological parameters obtained by the rheometer.

In order to record the exact moment of the flow restart, the visualization system is activated 10 seconds before the pump. The inlet pressure, the pressure drop, average flow rate, mean velocity, and temperature data are recorded and synchronized with the image acquisition system. The pressure data are recorded until 1000 s after the image recording is stopped.

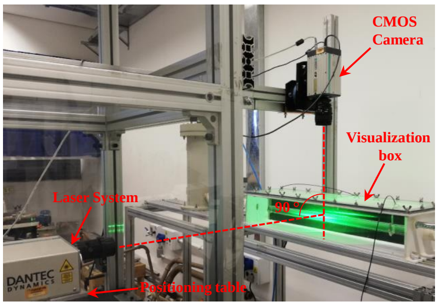

Figure 3: Visualization system setup. The plane of the laser beam and the visualization plane of the camera is set in a perpendicular configuration.

3. METHODOLOGY VALIDATION

The PIV methodology in transient regime flows was validated with a test performed with glycerine as Newtonian fluid. The velocity profiles were obtained for different pressure drop along the test section and compared with the analytical solution for unidirectional velocity in the transient flow regime given by Watson (1995), Eq. (3):

$$u(r,t) = \frac{R^2 \Delta p}{4 \mu L}\left[1 - \left(\frac{r}{R}\right)^2\right] - \sum_{n=0}^{\infty} C_n J_0(\lambda_n r) e^{-\lambda_n \frac{\nu t}{R^2}} \tag{3}$$

where Δp is the pressure drop between two points along the test section with a distance (L), (R) is the radius of the pipe, (μ) is the dynamic viscosity, (ν) the kinematic viscosity, (r) radius, (J_0) and (J_1) are the zero and first Bessel function, respectively. The (λ_n) variable represents the eigenvalues calculated for the respectively Bessel functions, and (t) is variable of time. The coefficients C_n are expressed as:

$$C_n = \frac{8R^2}{\lambda_n^3 J_1(\lambda_n)} \tag{4}$$

Figure 4 shows the comparison of the velocity profiles obtained by the flow visualization with the analytical profiles obtained by Eq. (3) at different times for a Re =1 and pressure drop of 911 Pa.

The validation stage shows that despite the refinement limitations of PIV technique at the wall region, the methodology used has a good agreement with the analytical solution for Newtonian fluid flows in straight pipes for different instants of time.

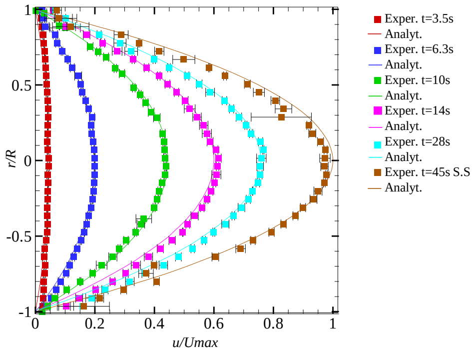

Figure 4: Velocity profiles obtained for a Re =1 and pressure drop of 911 Pa by PIV technique in transient regimen and compared with the analytical velocity solution for a Newtonian fluid, Eq. (3).

4. RESULTS AND DISCUSSION

The results below will be present the profiles velocity, the deformation maps, the evolution of shear stress over time, and the behavior of the wall slip velocity as a function of the shear stress, for Carbopol 20 wt% and 30 wt% for different Reynolds.

4.1 Profiles velocity

The velocity profile was obtained using the PIV technique and the help of a software to correlate the images obtained. By correlating the seeding particles set in motion from rest, the vector map was calculated for each position of the particle in the test section. Then, from this vector map, the mean axial velocity and shear maps were calculated.

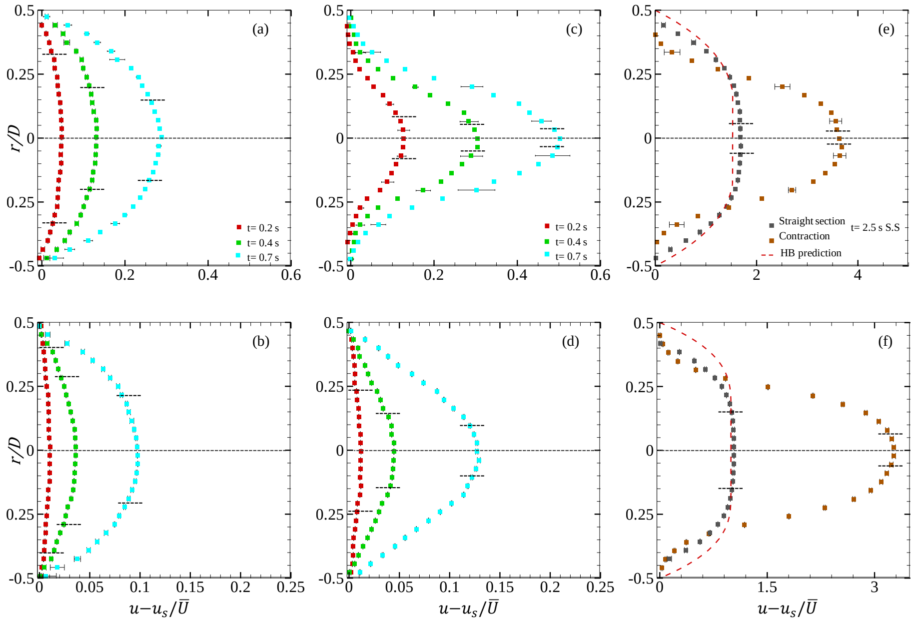

Figure 5: Dimensionless axial velocity $u/\bar{U}$ for two geometries, using Re =10 and corrected for the slip velocity u_s. They are plotted for three times (t_1=0.2s, t_2=0.4s, t_3=0.7s) and the steady-state ($t_{s.s}$=2.5s). the y-axis is the dimensionless radius by the diameter. The velocity profiles for Carbopol 20 wt% are shown in Fig. 5: a) straight section, c) abrupt contraction, and e) steady-state. The results for Carbopol 30 wt% are shown in Fig. 5: b) straight section, d) abrupt contraction, and f) steady-state. The black dashed line represent de plug core diameter. The red dashed line in Fig. 5e and Fig. 5f is the steady-state velocity profile predicted by the HB model.

The axial velocity profiles (u-u_s) as a function of radial position r, for Carbopol 20 wt% and 30 wt% were made dimensionless by the mean velocity ($\bar{U}$) taken from the mass flow meter. Here u is the velocity determined from the PIV data and u_s is the slip velocity at the wall of the pipe, determined by averaging the fitted values at the walls on the two sides of the velocity profile. The (u-u_s) for a Re =10 are showed in Fig. 5 for three different times during start-up flow and for steady state. Initially, it is observed that for t_1=0.2s, the velocity profile for Carbopol 20 wt% in the straight section (Fig. 5 a) and in the abrupt contraction (Fig. 5 c) presents some irregular and asymmetric regions, probably related to the fact that in the first moments the propagation of the pressure is not uniform and the breakdown of the material has not occurred (Mitishita *et al.*, 2018). In the other hand, the shear stress is less than the yield stress, and it is possible that the material responds elastically to the pressure imposed. For t_1 the black dashed lines indicate the formation of plug core, which is also observed for Carbopol 30 wt% in the two geometries (Fig. 5 b and Fig. 5 d). Subsequently, it is observed that for t_2=0.4s y t_3=0.7s the experimental velocity profile for Carbopol 20 wt% and 30 wt% in both geometries presents a greater destructuring and the experimental velocity profile at steady-state (Fig. 5 e,f) was close to the plug flow predicted by the HB model (Eq. (5)), with an experimental error of 9.42% for 20 wt% and 4.24% 30 wt%. It is also observed that the size of plug core increases with the yield stress, since the higher values τ_y present larger areas without yielding in the flow structure. This means that for the first instants of the start-up flow, the structure of the plug core is greater as observed in t_1, where the external forcing (the applied stress in our experiments) is greater to initiate the breakdown of material, but decreases as the destructuring of fluid advances (t_2, t_3).

$$u_z = \frac{nR}{n+1}\left(\frac{\tau_w}{k}\right)^{1/n}\left\{(1-\phi)^{\frac{(n+1)}{n}} - \left(\frac{r}{R}-\phi\right)^{\frac{(n+1)}{n}}\right\} \tag{5}$$

where n is the fluid index, k is the consistency index, τ_w is the wall shear stress, r is the radius, R is the radius of the pipe, and ϕ is the ratio $\frac{\tau_y^H}{\tau_w}$ for the Herschel Bulkley case.

The ratio u-$u_s/\bar{U}$ for Re =10, reaches at t_3 a value of 0.1 for 30 wt% (Fig. 5 b) and 0.27 for 20 wt% (Fig. 5 a) that is two order of magnitude greater than 0.1 at the straight section. For this value of u-$u_s/\bar{U}$ the radius of plug core (r_p) for each fluid is 0.15D for 20 wt% and 0.24D for 30 wt%, and represents near 30% and 48% of the entrance area section. For the abrupt contraction the u-$u_s/\bar{U}$ takes values of 0.5 and 0.13 for Carbopol 20 wt% and 30 wt% respectively, and of r_p represents the 8% and 20% of the entrance area section. Therefore, as the Reynolds number reaches higher values, the r_p is reduced and the time requiered for the destructuring of fluid is less, as shown below for a Re =100 (Fig. 6).

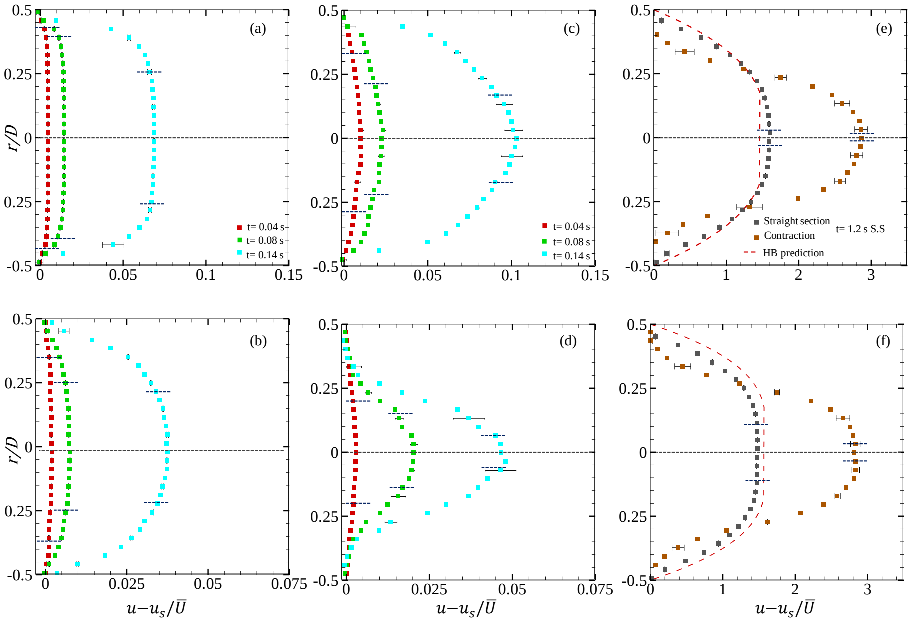

Figure 6: Dimensionless axial velocity $u/\bar{U}$ for two geometries, using Re =100 and corrected for the slip velocity u_s. They are plotted for three times (t_1=0.04s, t_2=0.08s and t_3=0.14s) and the steady-state ($t_{s.s}$=1.2s). the y-axis is the dimensionless radius by the diameter. The velocity profiles for Carbopol 20 wt% are shown in Fig. 6: a) straight section, c) abrupt contraction, and e) steady-state. The results for Carbopol 30 wt% are shown in Fig. 6: b) straight section, d) abrupt contraction, and f) steady-state. The black dashed line represent de plug core diameter. The red dashed line in Fig. 6e and Fig. 6f is the steady-state velocity profile predicted by the HB model.

Fig. 6 shows the velocity profiles of Carbopol at 20% by weight and at 30% by weight for Re = 100. Initially, at t_1=0.04ss, the asymmetric profiles and the formation of the core of the plug are also observed in the straight section (Fig. 6 a,b) and in abrupt contraction (Fig. 6 c,d). However, it is observed that for Re = 100 the external forcing is greater and the motion of the rigid body of the non-yielded fluid of the nucleus is less compared to Re = 10, that is, for a lower external forcing, the shear stress in the wall cannot exceed the yield stress of fluid and the size of plug core does not show a change in its structure for a longer time. Therefore, the higher the Reynolds number, the plug core appears early, the material destructuring time is shorter, and r_p decreases. This statement can be confirmed by comparing the Carbopol 20 wt% for two approximate times t_1=0.2s and t_3=0.14s in the straight section for Re =10 and Re =100 , it is observed that the r_p is 0.268D and 0.25D, respectively, representing 53.6% and 50% of the test section area for each time. On the other hand, it is again observed that due to the Carbopol 20 wt% has a lower yield stress, the ratio u-$u_s/\bar{U}$ is twice greater than compared to the Carbopol 30 wt% in both geometries. The steady-state velocity profiles for the two fluids and the two geometries are plotted and compared with the analytical solution of the HB model in Fig. 6 e,f. A good agreement is observed between the experimental profile and the analytical solution, with an experimental error of 8.27% and 6.32% for Carbopol 20 wt% and 30 wt%, respectively.

For the two concentrations of Carbopol and for the Reynolds numbers analyzed, it was observed that the velocity in the abrupt contraction is twice greater in the straight section, and this is due to the fact that the fluid is under large velocity gradients, and the slip velocity is lower in this geometry. The velocity profiles plotted for Carbopol 20 wt% Re =10 and Re =100, the slip velocity in the straight section and in the contraction represents 22.3% and 8.2% of the total velocity at the center of the pipe. In the case of Carbopol 30 wt%, this percentage was 24% and 3.48%. In the following sections, the behavior of u_s at each time will be discussed in function of shear stress.

4.2 Deformation Map

For simplicity, the deformation maps are shown for one case of Reynolds number to compare the two fluids. The deformation at a point is derived from the velocity gradient, which is estimated by comparing neighboring vectors with each other. A central difference scheme is used, and the resulting gradient corresponds to the slope of a 2^{nd} polynomial (i.e. parabolic) fit to three neighboring velocities, and therefore with 2^{nd} accurate. Then the gradient at the point (m, n) of the velocity component U in the direction x will be calculated as follows:

$$\frac{\partial U}{\partial x}(m,n)_{Central} \cong \frac{U_{m+1n} - U_{m-1n}}{x_{m+1n} - x_{m-1n}} = \frac{U_{m+1n} - U_{m-1n}}{2\Delta x} \qquad (6)$$

Figure. 7 shows the deformation maps for Carbopol 20 wt% and 30 wt% using Re =10 dimensioned by the apparent shear rate ($\dot{\gamma}_{aw}$) calculated as a function of flow rate by Eq. (7). Comparing the evolution of the velocity profiles for the two fluids at t_1=0.2s for the straight section (Fig. 5a and Fig. 5b) with the results shown in Fig. 7a and Fig. 7i, it is initially observed that for low shear stress values (τ<τ_y), an elastic solid regime characterized by constant rates of material deformation (Putz and Burghelea, 2009; Divoux *et al.*, 2011), where the stress of the solid regime is practically unresponsive to the rate of forcing, and it probably reflects the local force of the gel structure. Then, non-uniform breaks of gel are evidenced, indicating that a destructuring process is taking place. For the abrupt contraction, the deformations of Carbopol 20 wt% are higher, as observed in Fig. 7e when compared to Fig. 7m, Carbopol 30 wt%. This is due to the geometry of the section where high velocity gradients are created, for longer times the deformations increase as explained below. Furthermore, the initial destructuring process in both geometries and the elastic effects present are affected by the applied external forcing, which varies with the Reynolds number.

$$\dot{\gamma}_{aw} = \frac{4Q}{\pi D} \tag{7}$$

where Q is the flow rate and D is the diameter of the pipe.

Figure 7b and Fig. 7j, show of the alternation of the elastic effects (t_2=0.4s), between approximately at r/D =0.20 and r/D=0.45. It is observed that the transition from the solid (plug-like) to the viscous state is not direct, is mediated by an intermediate deformation regime, that is, the applied shear stress is less than the yield stress, but the yield stress is less than the shear stress after destructuring, and according to (Putz and Burghelea, 2009; Poumaere *et al.*, 2014) the rheological behavior of material is not that of a Hookean solid (the deformation increases non-linearly with the applied stresses) and neither is that of a viscous fluid, as observed in the deformartion map. At the same time, it is observed that the dimensionless value of the deformation for the fluid 20 wt% is higher compared to 30 wt%, which is expected because its yield stress is lower. This is not only observed in the straight section, in the abrupt contraction is more evident due to the high shear rates generated by the area reduction (Fig. 7f and Fig. 7n).

Figure 7c and Fig. 7k show the flow in a more viscous state at t_3=0.7s, near to the steady-state, but irregularities and regions are still observed even without deformation between 0.25D and 0.30D, in the same way, it is observed in the abrupt contraction (Fig. 7g and Fig. 7o), but higher values of deformartion were reached between X/D =0 and X/D =0.25, being more noticeable for 20 wt%. Finally, the deformation map and the axial velocity profile for steady-state flow at t=2.5s were obtained by the statistical mean of the data acquired 10 s after the detection of fluid movement, using 300 images.

It is possible to observe that the magnitude of the deformation is directly proportional to the velocity at which the fluid is forced. In other words, the linear increase in deformation is a direct consequence of varying the applied stress linearly. In the next section, the evolution of shear stress over time will be analyzed.

4.3 Wall shear stress

The results of the tests using Carbopol 20 and 30 wt % for Re =10 are presented. The inlet pressure (P_i) and wall shear stress τ_w, calculated using Eq. (8) and shown in Fig 8a,b. In this experiment, the imposition of flow rate started at t=0.1s, time for which P_i and τ_w initially suddenly increased, and then close to t=1.5s reached stable values. The black dashed line in P_i is the linear adjustment made before and after τ_w began to stabilize ($0 < t < 1s$ and $1.2 < t < 2.5s$). The lines intersect at t^* and then it was designate τ_w^* to be the value of τ_w at that point. For Carbopol 20 wt% τ_w^*=1.34 Pa and for Carbopol 30 wt% it is 3.8 Pa, these shear stress values were six and three greater than τ_y calculated by rheometer tests.

$$\tau_w = \frac{D\Delta p_{1-2}}{4L_{1-2}} \tag{8}$$

here D is the diameter, Δp_{1-2} is the difference between the two pressure measurement points (inlet P_i and outlet P_o pressure), and L the length between the pressure sensor at the inlet and outlet of the test section.

Fig 8c,d shows the evolution of P_i and τ_w as a function of time for the same fluids using Re =100. As in the experiment with $Re = 10$, a sudden increase in both P_i and τ_w is observed ($0 < t < 0.3s$), followed by a stabilization of the values ($0.48s < t < 1.2s$). The sudden increase in P_i and τ_w is due to the fact that in the first moments of start-up flow a greater pressure is required to break the gel-like structure, immediately after a subtle pressure drop is observed, followed by a time interval until reaching stable values. The τ_w^* value at t^* considerably exceeds the τ_y calculated in the rheometer and is also greater than that obtained for Re =10, this is due to the fact that the shear stress increases with the Reynolds number.

The two experiments shown in Fig 8 show that for low and higher Reynolds number the τ_w exceeded the yield stress, breaking the material structure, at the same time it was observed that the higher the Reynolds imposed, the time required to exceed the yield stress is low. These results contrast with those obtained by Liu and de Bruyn (2018), where it is shown that for the experiments carried out on smooth pipes for low forcing rates, the τ_w was substantially less than the yield stress calculated in rheometric tests. An explanation for this discrepancy in the results may be due to the long forcing times applied and the rheological properties of the materials studied.

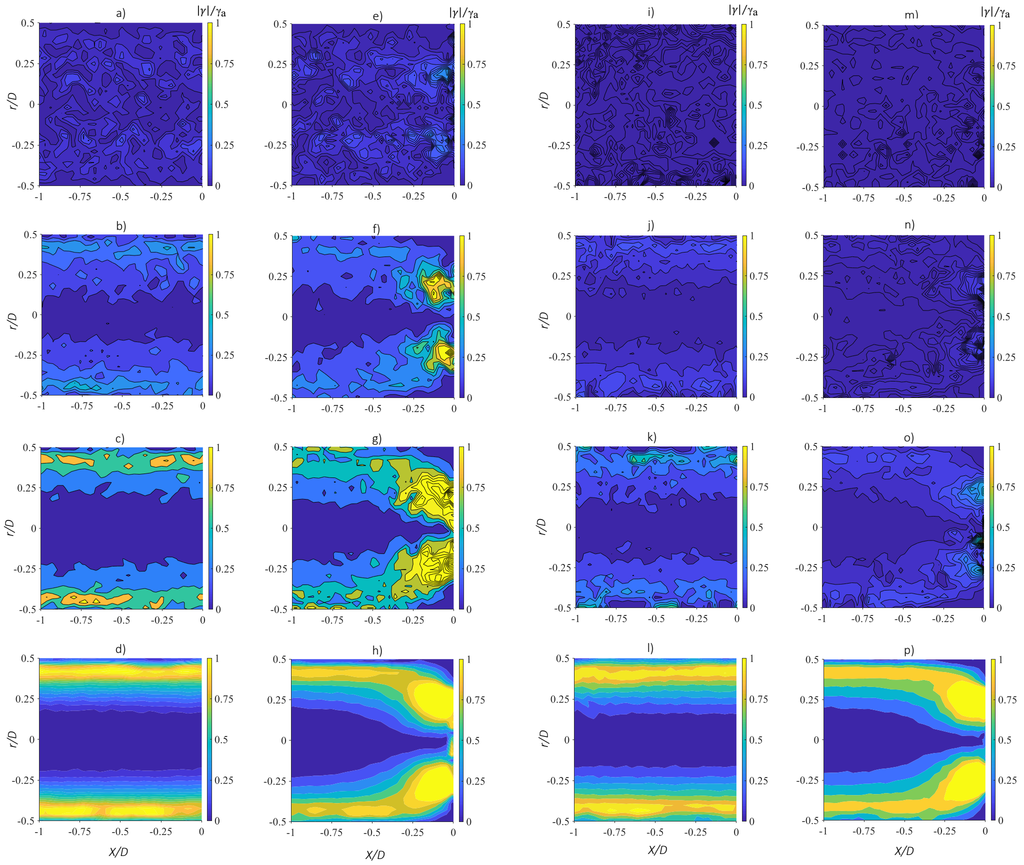

Figure 7: Dimensionless deformation maps for ($\dot{\gamma}_{aw}$) using Re =10 in straight section for Carbopol 20 wt %: a), b), c) and d). Carbopol 30 wt %: i), j), k) and l). Abrupt contraction, Carbopol 20 wt %: e), f), g) and h). Carbopol 30 wt %: m), n), o) and p).

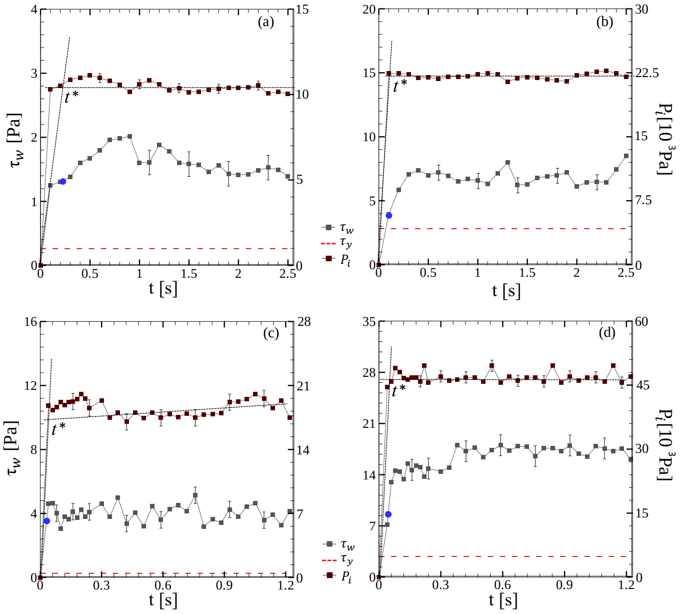

Figure 8: Time evolution of inlet pressure (P_i) and shear wall stress (τ_w) for Re = 10 a) Carbopol 20 wt%, b) Carbopol 30 wt%, and Re = 100 c) Carbopol 20 wt% and d) Carbopol 30 wt%. The time at which the two fits intersect is t^*. The wall shear stress τ_w, calculated from Eq. (8). The blue circle is $\tau_w{}^*$, the wall shear stress at t^*. The dashed line is the yield stress measured with the rheometer. The uncertainty of τ_w and P_i are shown by the error bars.

4.4 Slip velocity behavior

The yielding transition of yield stress fluids is often associated to wall slip conditions which affects the start-up process and flow behavior. The effect of the slip velocity on the total velocity at the center of the pipe was analyzed for two fluids used and Re =10. Fig. 5a and Fig. 5b showed the velocity profiles for Carbopol 20 wt% and 30 wt% in the straight section. It was observed that the slip velocity (u_s) represented 22%, 4.5%, 3.80% and 48% of total velocity in the center of the pipe (u-u_s) for t_1, t_2, t_3 and steady-state (Fig. 5e), respectively. In contrast u_s for Carbopol 30 wt% represented 7.38%, 5.72%, 3.04% of u-u_s for the transient time and 71.6% in steady state. For the case of the abrupt contraction and the fluid 20 wt% (Fig. 5c and Fig. 5d) u_s represent 7.38%, 0.98%, 0.59%, and 2.72% for the steady-state of u-u_s. For the same geometry and using the 30 wt% fluid, u_s were 2.48%, 1.79%, 9.17% in the three times analyzed, and 0.13% for the steady-state flow (Fig. 5f). This first part of analysis shows that the slip velocity is higher in the straight section, compared to the abrupt contraction at all times, and finally, it presents an unstable behavior in the transient interval and increasing again in the steady-state for both geometries.

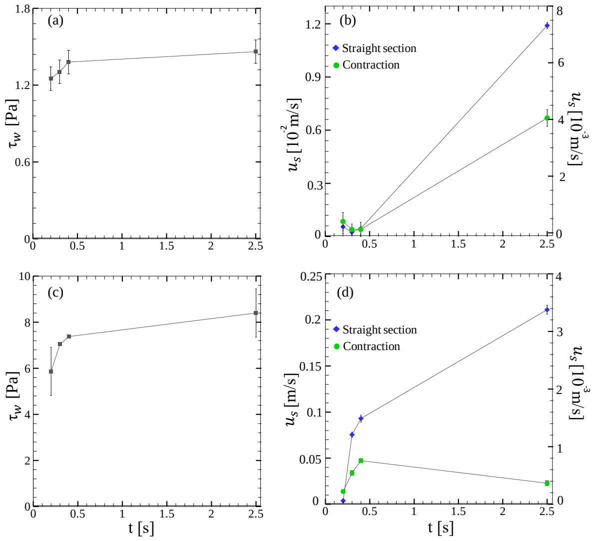

Figure 9: a) Evolution of the wall shear stress b) and the slip velocity for t_1, t_2, t_3 and steady-state ($t_{s.s}$) for Carbopol 20 wt% and Re =10. The results for Carbopol 30 wt% are shown in c) and d). The error bars indicate the average of the data in the analyzed time. The measurement scale on the right and left indicate the u_s values for straight section and abrupt contraction, respectively.

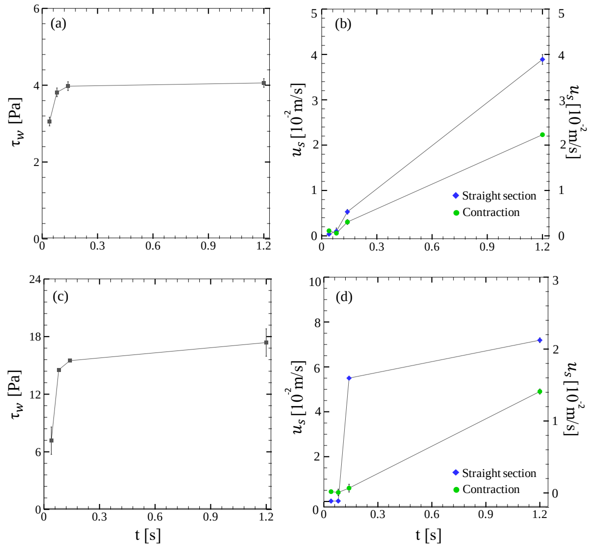

Figure 10: a) Evolution of the wall shear stress b) and the slip velocity for t_1, t_2, t_3 and steady-state ($t_{1.2s}$) for Carbopol 20 wt% and Re =100. The results for Carbopol 30 wt% are shown in c) and d). The error bars indicate the average of the data in the analyzed time.The measurement scale on the right and left indicate the u_s values for straight section and abrupt contraction, respectively).

The second part involved the analysis of the slip velocity for Re =100 and Carbopol 30 wt% (Fig. 6). It was observed that the slip velocity in the straight section for the two fluids was always greater than in the abrupt contraction, although curiously for t_1 in the contraction u_s it represented 33.1% of u-u_s, it is possible that this fact is related to the pressure oscillations produced in the first moments of the destructuring of the plug core in this region. Comparing the results of the two fluids for the two Reynolds in the two geometries it is found that u_s principally affects the total velocity for the straight section. A major static residual slip layer in the straight section is the answer to why slip velocity was perceived compared to the abrupt contraction (Taghavi *et al.*, 2012). However, although the slip velocity is lower in the abrupt contraction, due to the acceleration of the fluid in this region, the fact that this phenomenon is coupled to the yielding transition and its independent of the geometry cannot be ruled out.

Figure 9 shows the shear stress $\tau_w(t)$ and slip velocity $u_s(t)$ for Carbopol 20 and 30 wt% using Re =10 for the start-up flow times analyzed in the two geometries. Initially, it is observed that the shear stress in the wall increases for both fluids and that beyond the yield stress it continues to do so until a stabilization value is reached. The slip velocity also increases along with τ_w, as shown for the straight section and contraction, indicating a dependence with τ_w. However, for both fluids u_s the contraction is approximately one and three orders of magnitude less than the straight section. According to Nguyen and Boger (1992), u_s decreases beyond the yield stress, these results contrast with those obtained in this study, which indicate that the slip velocity continues to increase after the τ_w exceeds the yield stress of material.

Figure 10 shows $\tau_w(t)$ and $u_s(t)$ as a function of time for Re =100, again the findings indicate an increase in the slip velocity, with the applied shear stress, independent of the solid, fluid, or solid-fluid degree of deformation (Fig. 7). This conclusion is consistent with the experimental findings for the case of a constant pipe flow (Pérez-González *et al.*, 2012).

5. CONCLUSIONS

An experimental investigation on the transient yielding of two Carbopol® 940 solutions in pipe flow is presented by PIV technique. From results was possible obtain velocity data, from which velocity profiles were obtained for different times from start-up to fully developed condition in a horizontal straight pipe and a abrupt contraction configuration. The visualization of start-up flow allowed to identify some mechanisms present during the restarting flow of a viscoplastic fluid. It was observed the existence of different phases during the start-up regardless of the geometry. The first phase is characterized by an elastic behavior, which indicates that during the yielding of viscoplastic fluids, the influence of elastic effects during the solid-fluid transition cannot be ignored. Then, after the yield stress of material is exceeded. It is observed a coexistence of solid and liquid phases, in which the fluid offered resistance for flowing, and a oscillation between the destructuring and structuring of the material is presented. It is also observed that in the coexistence of phases, the wall shear stress increases with the Reynolds number, and proportional to this increase, the effects of wall slip, observing larger non-yielding areas and core un-yielded fluid movements. Furthermore, the time and space measurements of the flow fields based on the PIV technique allowed us to attempt to provide an experimental characterization of the wall slip phenomenon, revealing coupling between the irreversible solid-fluid transition and the slip phenomenon. Finally, the fluid exhibited steady-state flow that is well-described by the predictions of the Herschel–Bulkley model.

6. ACKNOWLEDGEMENTS

This work has been supported by the Federal University of Technology-Parana's Research Center for Rheology and Non-Newtonian Fluids-CERNN and Multilab LabReo-CERNN/UTFPR

7. REFERENCES

Alba, K. and Frigaard, I., 2016. "Dynamics of the removal of viscoplastic fluids from inclined pipes". *Journal of Non-Newtonian Fluid Mechanics*, Vol. 229, pp. 43–58.

Benmouffok-Benbelkacem, G., Caton, F., Baravian, C. and Skali-Lami, S., 2010. "Non-linear viscoelasticity and temporal behavior of typical yield stress fluids: Carbopol, xanthan and ketchup". *Rheologica acta*, Vol. 49, No. 3, pp. 305–314.

Burfoot, D., Middleton, K. and Holah, J., 2009. "Removal of biofilms and stubborn soil by pressure washing". *Trends in Food Science & Technology*, Vol. 20, pp. S45–S47.

Cole, P.A., Asteriadou, K., Robbins, P.T., Owen, E.G., Montague, G.A. and Fryer, P.J., 2010. "Comparison of cleaning of toothpaste from surfaces and pilot scale pipework". *Food and bioproducts processing*, Vol. 88, No. 4, pp. 392–400.

Coussot, P., 2014. "Yield stress fluid flows: A review of experimental data". *Journal of Non-Newtonian Fluid Mechanics*, Vol. 211, pp. 31–49.

Coussot, P. and Meunier, M., 1996. "Recognition, classification and mechanical description of debris flows". *Earth-Science Reviews*, Vol. 40, No. 3-4, pp. 209–227.

Curran, S., Hayes, R., Afacan, A., Williams, M. and Tanguy, P., 2002. "Properties of carbopol solutions as models for yield-stress fluids". *Journal of Food Science*, Vol. 67, No. 1, pp. 176–180.

Dalla, L.F., Soares, E.J. and Siqueira, R.N., 2019. "Start-up of waxy crude oils in pipelines". *Journal of Non-Newtonian Fluid Mechanics*, Vol. 263, pp. 61–68.

Divoux, T., Barentin, C. and Manneville, S., 2011. "From stress-induced fluidization processes to herschel-bulkley behaviour in simple yield stress fluids". *Soft Matter*, Vol. 7, No. 18, pp. 8409–8418.

El-Gendy, H., Alcoutlabi, M., Jemmett, M., Deo, M., Magda, J., Venkatesan, R. and Montesi, A., 2012. “The propagation of pressure in a gelled waxy oil pipeline as studied by particle imaging velocimetry”. *AIChE journal*, Vol. 58, No. 1, pp. 302–311.

Fernandes, R.R., Turezo, G., Andrade, D.E., Franco, A.T. and Negrão, C.O.R., 2019. “Are the rheological properties of water-based and synthetic drilling fluids obtained by the fann 35a viscometer reliable?” *Journal of Petroleum Science and Engineering*, Vol. 177, pp. 872–879.

Fryer, P., Christian, G. and Liu, W., 2006. “How hygiene happens: physics and chemistry of cleaning”. *International Journal of Dairy Technology*, Vol. 59, No. 2, pp. 76–84.

Huilgol, R.R., Alexandrou, A.N. and Georgiou, G.C., 2019. “Start-up plane poiseuille flow of a bingham fluid”. *Journal of Non-Newtonian Fluid Mechanics*, Vol. 265, pp. 133–139.

Liu, Y. and de Bruyn, J.R., 2018. “Start-up flow of a yield-stress fluid in a vertical pipe”. *Journal of Non-Newtonian Fluid Mechanics*, Vol. 257, pp. 50–58.

Malin, M., 1998. “Turbulent pipe flow of herschel-bulkley fluids”. *International communications in heat and mass transfer*, Vol. 25, No. 3, pp. 321–330.

Mitishita, R.S., Oliveira, G.M., Santos, T.G. and Negrão, C.O., 2018. “Pressure transmission in yield stress fluids-an experimental analysis”. *Journal of Non-Newtonian Fluid Mechanics*, Vol. 261, pp. 50–59.

Møller, P., Fall, A. and Bonn, D., 2009. “Origin of apparent viscosity in yield stress fluids below yielding”. *EPL (Europhysics Letters)*, Vol. 87, No. 3, p. 38004.

Møller, P.C., Mewis, J. and Bonn, D., 2006. “Yield stress and thixotropy: on the difficulty of measuring yield stresses in practice”. *Soft matter*, Vol. 2, No. 4, pp. 274–283.

Nguyen, Q. and Boger, D., 1992. “Measuring the flow properties of yield stress fluids”. *Annual Review of Fluid Mechanics*, Vol. 24, No. 1, pp. 47–88.

Ovarlez, G., Cohen-Addad, S., Krishan, K., Goyon, J. and Coussot, P., 2013. “On the existence of a simple yield stress fluid behavior”. *Journal of Non-Newtonian Fluid Mechanics*, Vol. 193, pp. 68–79.

Pérez-González, J., López-Durán, J.J., Marín-Santibáñez, B.M. and Rodríguez-González, F., 2012. “Rheo-piv of a yield-stress fluid in a capillary with slip at the wall”. *Rheologica acta*, Vol. 51, No. 11-12, pp. 937–946.

Phillips, D.A., Forsdyke, I.N., McCracken, I.R. and Ravenscroft, P.D., 2011. “Novel approaches to waxy crude restart: Part 2: An investigation of flow events following shut down”. *Journal of Petroleum Science and Engineering*, Vol. 77, No. 3-4, pp. 286–304.

Poumaere, A., Moyers-González, M., Castelain, C. and Burghelea, T., 2014. “Unsteady laminar flows of a carbopol® gel in the presence of wall slip”. *Journal of Non-Newtonian Fluid Mechanics*, Vol. 205, pp. 28–40.

Putz, A.M. and Burghelea, T.I., 2009. “The solid–fluid transition in a yield stress shear thinning physical gel”. *Rheologica Acta*, Vol. 48, No. 6, pp. 673–689.

Roberts, G.P. and Barnes, H.A., 2001. “New measurements of the flow-curves for carbopol dispersions without slip artefacts”. *Rheologica Acta*, Vol. 40, No. 5, pp. 499–503.

Sierra, A.G., Varges, P.R. and Ribeiro, S.S., 2016. “Startup flow of elasto-viscoplastic thixotropic materials in pipes”. *Journal of Petroleum Science and Engineering*, Vol. 147, pp. 427–434.

Taghavi, S., Alba, K., Moyers-Gonzalez, M. and Frigaard, I., 2012. “Incomplete fluid–fluid displacement of yield stress fluids in near-horizontal pipes: experiments and theory”. *Journal of Non-Newtonian Fluid Mechanics*, Vol. 167, pp. 59–74.

Watson, G.N., 1995. *A treatise on the theory of Bessel functions*. Cambridge university press.

8. RESPONSIBILITY NOTICE

The following text, properly adapted to the number of authors, must be included in the last section of the paper: The author(s) is (are) solely responsible for the printed material included in this paper.